



Article

Computational Analysis of Premixed Syngas/Air Combustion in Micro-channels: Impacts of Flow Rate and Fuel Composition

Sunita Pokharel ¹, Mohsen Ayoobi ^{2,*}  and V'yacheslav Akkerman ¹ 

¹ Center for Innovation in Gas Research and Utilization (CIGRU), Department of Mechanical and Aerospace Engineering, West Virginia University, Morgantown, WV 26506, USA; sp0078@mix.wvu.edu (S.P.); vyacheslav.akkerman@mail.wvu.edu (V.A.)

² Division of Engineering Technology, Wayne State University, Detroit, MI 48202, USA

* Correspondence: mohsen.ayoobi@wayne.edu

Abstract: Due to increasing demand for clean and green energy, a need exists for fuels with low emissions, such as synthetic gas (syngas), which exhibits excellent combustion properties and has demonstrated promise in low-emission energy production, especially at microscales. However, due to complicated flame properties in microscale systems, it is of utmost importance to describe syngas combustion and comprehend its properties with respect to its boundary and inlet conditions, and its geometric characteristics. The present work studied premixed syngas combustion in a two-dimensional channel, with a length of 20 mm and a half-width of 1 mm, using computational approaches. Specifically, a fixed temperature gradient was imposed at the upper wall, from 300 K at the inlet to 1500 K at the outlet, to preheat the mixture, accounting for the conjugate heat transfer through the walls. The detailed chemistry of the ignition process was imitated using the San Diego mechanism involving 46 species and 235 reactions. For the given boundary conditions, stoichiometric premixed syngas containing various compositions of carbon monoxide, methane, and hydrogen, over a range of inlet velocities, was simulated, and various combustion phenomena, such as ignition, flame stabilization, and flames with repeated extinction and ignition (FREI), were analyzed using different metrics. The flame stability and the ignition time were found to correlate with the inlet velocity for a given syngas mixture composition. Similarly, for a given inlet velocity, the correlation of the flame properties with respect to the syngas composition was further scrutinized.

Keywords: micro-combustion; syngas; repetitive extinction and ignition (FREI); numerical simulations; flame instabilities



Citation: Pokharel, S.; Ayoobi, M.; Akkerman, V. Computational Analysis of Premixed Syngas/Air Combustion in Micro-channels: Impacts of Flow Rate and Fuel Composition. *Energies* **2021**, *14*, 4190. <https://doi.org/10.3390/en14144190>

Academic Editor: Giuseppe Pascazio

Received: 13 June 2021

Accepted: 7 July 2021

Published: 11 July 2021

Publisher's Note: MDPI stays neutral with regard to jurisdictional claims in published maps and institutional affiliations.



Copyright: © 2021 by the authors. Licensee MDPI, Basel, Switzerland. This article is an open access article distributed under the terms and conditions of the Creative Commons Attribution (CC BY) license (<https://creativecommons.org/licenses/by/4.0/>).

1. Introduction

Due to expanding interest in and development of cutting-edge, highly-effective miniaturized and portable power generation devices, such as unmanned aerial vehicles (UAVs), microsatellite thrusters, miniature reactors, and sensors, the demand exists for more advanced technologies with reduced weight and high durability. Further, the combination of heat and power microsystems and thermo-photovoltaic applications, in which micro-combustion systems play a significant role, is advancing [1,2]. Although new energy resources such as batteries are emerging rapidly, they still have considerably lower energy densities compared to combustion-based sources [3]. In particular, the density of the energy stored in a typical hydrocarbon fuel is orders of magnitude higher than that in a typical lithium-ion battery [4]. Therefore, combustion-based power generation cannot be phased out immediately, especially in aviation and aerospace applications, and other devices such as micro satellites, for which weight is a critical and deciding factor. Thus, because combustion has been and remains the most reliable energy source, due to the high energy density of fossil fuels [5,6], and due to the increasing need for clean, green, and sustainable (CGS) energy, a critical need exists for an efficient method to sustain such micro-combustion.

Regarding CGS energy and its compatibility with other power generation systems based on combustion, numerous studies have been conducted on the application of synthetic gas (syngas), and have proven that syngas is potentially more advantageous than conventional fuels [7], with advantages ranging from cheaper production to lower emissions [8]. Syngas is mainly produced through gasification of heavy hydrocarbons (C_xH_y), biomass, or coal-based feedstocks, with carbon dioxide (CO_2) eliminated from the environment. The composition of syngas also varies depending on the raw material and the production process [9–12]. For instance, it exhibits high adiabatic flame temperatures in the presence of hydrogen (H_2) and carbon monoxide (CO) [13]. Furthermore, the combination of H_2 and CO provides a lower flammability limit than methane (CH_4) and a higher upper limit than other hydrocarbons, having a wider flammability range than conventional fuels such as oil or natural gas. Thus, the presence of H_2 and CO in syngas exhibits flame-retardant characteristics, whereas the presence of inert gases such as nitrogen (N_2) and CO_2 reduces the flammability limits of syngas.

Regarding the unstretched laminar burning velocity, S_L , using a detailed chemical kinetics mechanism, Pio et al. [14] studied the effect of syngas composition on reactivity, adiabatic flame temperature, T_a , energy, and pollutant production rate. Comparing their work with the data from the literature, the authors of Ref. [14] found that the volumetric increment of CO_2 and CO reduced S_L , in addition to which the kinetic effect of CO_2 led the maximum values of S_L and T_a to shift towards the stoichiometric compositions. Syngas explosion properties in closed vessels and the impacts of different operating conditions, such as the equivalence ratio and syngas composition, on the flame characteristics have also been the subject of many studies [15–17]. The impact of H_2 -addition to CH_4 on the properties of syngas combustion was studied by Mardani et al. [18]. It was shown that H_2 -enrichment led to higher volumes of the hot regions and faster upstream movement, in addition to an increase in the distance between the locus of the maximum temperature and that of the stoichiometric mixture fraction, so that the maximum temperature exceeded the adiabatic flame temperature. Zhang et al. [19] studied the effect of fuel variability for high hydrogen-containing syngas and demonstrated a good performance of the combustion process for certain fractions of H_2 and CO. Further, the effects of CO_2 and N_2 at various equivalence ratios were compared by Dam et al. [20]. Similarly, the effect of varying syngas composition (based on different production methods) at different pressures was studied by Monteiro et al. [21]. Although all the studies listed above showed important contributions of different fuel components to the combustion properties, the systems of interest were very large compared to micro-combustors. Wei et al. [22] identified the operating cost as the major issue for syngas production, which was then suggested to have significantly reduced unit costs for higher production when industrialized with better manufacturing and optimization techniques. Research in this area is still in its rudimentary phases as burning at microscales and macroscales shows different behaviors [23–25]. Therefore, further research is critically needed to study syngas combustion at microscales.

In a microscale system, the surface area to the volume ratio is higher than that at larger scales, which promotes heat losses from the system [25–28], thereby reducing the efficiency of a combustor. Further, a smaller size of the system leads to a reduced characteristic length scale of the flow and, therefore, a lower Reynolds number. Consequently, the flow is laminar. Although experimental analysis of combustion at both conventional scales and microscales is essential to validate the computational or analytical models and results, numerical simulations allow researchers to minimize the investments in experimental trials; in particular, preliminary results from numerical simulations can help researchers be more objective with their experimental setup and analysis. In microscale and mesoscale combustors, the stabilizing and destabilizing effects of the flame stretch, due to the wall heat losses, further complicate the analysis.

Various studies have been conducted in the past to sustain the microscale combustion process by incorporating a bluff body and a cavity into a micro-combustor [29], and some researchers focused on the impact of the adiabatic walls on the flame stability in micro-

combustors [30]. In particular, Pizza et al. [31] conducted extensive numerical simulations to study the characteristics of H₂-air combustion in a two-dimensional (2D) channel, employing various channel heights and inlet velocities of a reactant. Further studies have been conducted for other fuels, such as methane (CH₄) [26,32,33], propane (C₃H₈) [34–36], and syngas [24,37,38]. The numerical work of Kousheshi et al. [39] also analyzed the effect of syngas composition on the engine exhaust, with the reduction of the ignition delay time, sharper heat release rate, more NO_x, and less soot, CO, and unburned hydrocarbon production obtained for an H₂-rich mixture. These computational findings on the flame instabilities have also been confirmed experimentally [40]. Brambilla et al. [24] studied lean-premixed, syngas-air combustion in a microchannel of 7 mm height, by varying the equivalence ratios in the range $0.35 \leq \phi \leq 0.42$, the volumetric CO:H₂ ratio from 1:1 to 20:1, and the wall temperatures from 550 to 1320 K. As a result, the steady V-shaped and asymmetric flames, with the stationary and oscillatory modes, were observed in this work. Further, the stable flames, in addition to the flames with repetitive extinction and ignition (FREI), were shown for CH₄-air burning in a microchannel of 2 mm diameter by Maruta et al. [41]. This experimental work investigated how the flame behavior depends on the equivalence ratio, identifying the stable flames for $\phi < 1.3$, and the FREI were observed for $1.3 < \phi < 1.5$. The flat and stationary flames, with the cyclic oscillatory and the FREI behavior, were also observed for CH₄-air and C₃H₈-air combustion in another study by Maruta et al. [23], with a fixed temperature gradient maintained at the channel wall. The phenomenon of repetitive extinction/ignition has been also observed in several other experimental studies for various fuels such as CH₄ [42,43] and ethane (C₂H₆) [44].

Although syngas combustion at microscales has been studied previously, comprehensive studies accounting for detailed chemistry are necessary at these scales to further scrutinize the combustion characteristics, and the impacts of the mixture composition and the flow rate on various properties of syngas combustion at such small scales.

The present work is a step in this direction. Specifically, stoichiometric premixed syngas combustion in a microscale 2D channel was simulated by means of a detailed San Diego mechanism [45], aiming to scrutinize the flame behavior for various mixture compositions and inlet velocities. The remainder of the manuscript is organized as follows: the methodology is explained in Section 2; various combustion phenomena, such as extinction and ignition, stabilization, and instabilities, are observed and scrutinized in Section 3; and the conclusions are summarized in Section 4.

2. Methodology

In the following, the governing equations, operating conditions, and metrics guiding the analyses and conclusions are elucidated.

2.1. Governing Equations

The governing equations are the general balance equations for mass, momentum, species, and energy, which read:

$$\frac{\partial \rho}{\partial t} + \nabla \cdot (\rho \vec{v}) = 0, \quad (1)$$

$$\frac{\partial}{\partial t} (\rho \vec{v}) + \nabla \cdot (\rho \vec{v} \vec{v}) = -\nabla p + \nabla \cdot (\bar{\bar{\tau}}) + \rho \vec{g} + \vec{F}, \quad (2)$$

$$\frac{\partial}{\partial t} (\rho Y_i) + \nabla \cdot (\rho \vec{v} Y_i) = -\nabla \cdot \vec{J}_i + R_i, \quad (3)$$

$$\rho C_p \frac{\partial T}{\partial t} + \rho C_p \vec{v} \nabla T = -\nabla q - \rho \sum_{i=1}^N C_{p,i} Y_i V_i - \sum_{i=1}^N h_i \Omega_i, \quad (4)$$

respectively. Here ρ is the density of the system, C_p is the specific heat at constant pressure, p is the static pressure, $\bar{\bar{\tau}}$ is the stress tensor, T is the temperature, \vec{g} and \vec{F} are the

gravitational and external body forces, respectively; and R_i is the net rate of production for the i th species in the chemical reactions. The local mass fraction of each species Y_i is predicted by solving the convection-diffusion equation for the i th species, and V_i , h_i and Ω_i are, respectively, the diffusion velocity, the specific enthalpy, and the net rate of production of the i th species, $i = 1 \dots N$, with the total number of species N . \vec{J}_i in Equation (3) represents the diffusion flux of the i th species due to the gradients of the concentration and temperature. Fick's law is employed to approximate mass diffusion due to the concentration gradient:

$$\vec{J}_i = -\rho D_{i,m} \nabla Y_i - D_{T,i} \frac{\nabla T}{T}. \quad (5)$$

Here, $D_{i,m}$ is the mass diffusion coefficient of the i th species in the mixture, and $D_{T,i}$ is the thermal diffusion (Soret) coefficient. The simulations were performed using the commercial CFD package Ansys FLUENT (version 18.2) [46], employing the finite-volume discretization method. The following model options were chosen in the Ansys FLUENT simulation setup: pressure-based coupling, absolute velocity formulation, laminar viscosity, and volumetric species transport model. In addition, the semi-implicit method for pressure-linked equations (SIMPLE) was used as a numerical scheme to solve the Navier–Stokes equations. The methods and models employed in this work are widely used and accepted in the literature.

2.2. Operating Conditions

The computational domain is a 2D channel of length 20 mm and half-width 1 mm, as schematically shown in Figure 1. It is noted that 2D simulations were preferred in this work because (i) with the large number of the cases simulated here, it would have been very challenging (in terms of time and computational resources) to use a 3D domain, and (ii) although considering 3D impacts could possibly provide further detail of the combustion characteristics, 2D simulations provide sufficient insights into the fundamental processes occurring in narrow channels [31–33]. Both extremes of the channel were open, and the pressure at the inlet and outlet was atmospheric. To save the computational cost twice, the upper half of the channel was imitated by imposing the axisymmetric boundary conditions at the lower wall. The upper wall was imposed with a temperature gradient such that the wall temperature grows linearly, from 300 K at the inlet to 1500 K at the outlet, to account for the conjugate heat transfer at the wall. The temperature gradient of 60 K/mm was selected to ensure relatively high exit temperature (1500 K), where auto ignition of the air/fuel mixtures downstream of the channel can be guaranteed. The inlet mixture flowed with a uniform velocity profile, with a constant temperature and no-slip boundary conditions at the wall. A uniform square mesh of cell size 0.05 mm and a time step of 10 μ s were used in all simulations. It is important for the grid resolution to sufficiently resolve the flame thickness. Although the flame thickness depends on the operating conditions, including fuel composition, it remains in the same order of magnitude (≈ 1 mm) for the different cases studied here. Correspondingly, the selected grid resolution ensures that the flames are resolved, with around 20 cells inside the thickness of the flame front.

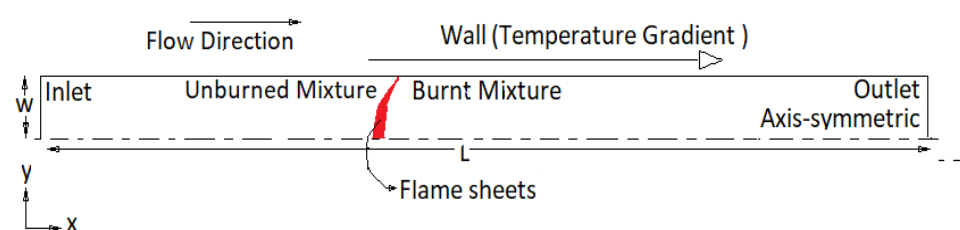


Figure 1. A schematic of the computational domain.

Stoichiometric premixed combustion of syngas comprised of CO, CH₄, and H₂ was considered, with three various mixture compositions, A, B and C, as listed in Table 1. Various inlet flow velocities were employed, from 0.1 to 3.0 m/s. To calculate the mass fractions of the species at the inlet, the following global mechanism of syngas combustion was used:

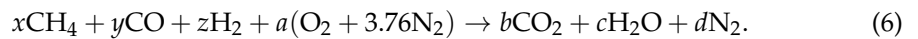


Table 1. The syngas mixture compositions studied in this work.

$x\text{CH}_4 + y\text{CO} + z\text{H}_2 + a(\text{O}_2 + 3.76\text{N}_2) \rightarrow \text{Products}$			
Fuel Mixture	$x(\%)$	$y(\%)$	$z(\%)$
A	30	5	65
B	70	5	25
C	60	10	30

The indexes x , y , and z in Equation (6) represent the fuel composition, and the coefficients a , b , c , and d are defined as:

$$a = \frac{4x + y + z}{2}, \quad (7)$$

$$b = x + y, \quad (8)$$

$$c = 2x + z, \quad (9)$$

$$d = 3.76 \left(\frac{4x + y + z}{2} \right). \quad (10)$$

The chemical kinetics obeys the San Diego mechanism with 46 species and 235 reactions [45].

2.3. Resolution Test

To verify the accuracy of the simulations and to ensure that the results do not depend on the grid size or time steps, two different resolution tests, for the grid and time resolutions, respectively, were performed and analyzed as described below.

Grid Resolution. The numerical simulation tool that was used in this work, Ansys FLUENT, is based on a finite-volume discretization, where the small volumes, also regarded here as mesh elements, play a very important role in accurately mimicking the physical phenomena and producing the effective results. The optimum mesh size needs to be chosen to obtain accurate results by nevertheless utilizing as minimal resources as possible. Because 2D simulations were of interest in this work, the simulation domain was discretized with an evenly sized square grid. Numerical simulations were performed over three different grid sizes: 0.02 mm (fine), 0.05 mm (moderately fine), and 0.1 mm (coarse), with all other conditions kept identical. To evaluate the simulation performance over these three grid sizes, the time evolution of the total heat release rate (HRR_T) is compared for all cases (see Figure 2). It is observed that although HRR_T experiences some variations depending on the mesh size, the ignition time (the time when HRR_T peaks), determining most of the combustion parameters, is practically the same for all three meshes. However, the time it took the software to complete the simulations almost doubled and the memory usage by the simulation almost tripled as the mesh size was refined from 0.1 to 0.05 mm, and from 0.05 to 0.02 mm. As expected, the results of the simulations with the finest mesh size (0.02 mm) were smoother compared to those with other two mesh sizes. Considering the number of simulations needed for this study, to more efficiently use time and memory resources, the moderately fine mesh size (0.05 mm) was chosen for all the simulations.

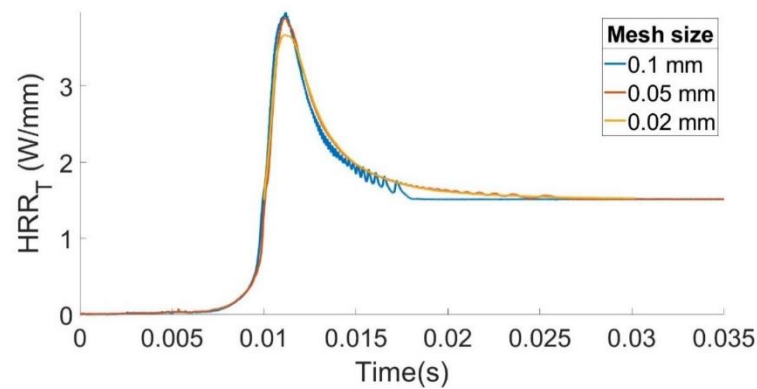


Figure 2. The grid resolution test for mixture A with the inlet velocity of 1.0 m/s.

Time Resolution. Due to the transient nature of the simulations in this work and, in particular, the significant variation of most properties with time, it was important to ensure that the results were not affected by the selected time step. Therefore, a baseline case was first simulated with various time steps (1, 10, and 50 μ s), while all other conditions were kept identical. Similar to the grid resolution test, the time evolution of HRR_T was compared for all time steps; see Figure 3. The results suggest that the time step of 50 μ s does not allow predicting the ignition time as accurately as the cases of smaller time steps (10 and 1 μ s), whereas the difference is minor when comparing the results associated with the time steps of 10 and 1 μ s. Again, to be most efficient with the time and memory resources, and to avoid sacrificing accuracy, the time step of 10 μ s was selected for all the simulations.

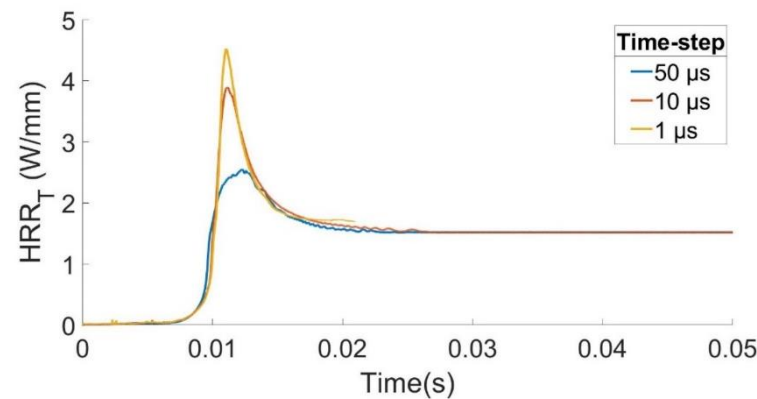


Figure 3. The time resolution test for mixture A with the inlet velocity of 1.0 m/s.

It is noted that there are no experimental results in the literature for the operating conditions, used in this paper, against which the results of this work could be compared. However, similar behavior (such as ignition process or FREI) observed in the literature [20,23,25,30,42–44] for different fuels and operating conditions, in addition to the resolution tests conducted here, confirm that the simulation results of this work are physically possible and valid. Therefore, the findings of this work could inspire future experiments, while being used as a guidance to design and perform such experiments.

2.4. Metrics

To scrutinize various combustion properties from the raw simulation data, the following metrics are introduced:

Heat release rate (HRR): This is a local property in the system, and is calculated by obtaining the summation of the net heat release rates for all the reactions involved in each computation cell. Due to the implementation of detailed chemistry in this work, comprehensive information about all species and reactions is available. Because the heat

release rate integrates the impact of all species and reactions into one parameter, and it is known to peak at the flame front, this was chosen as the most precise criterion to demarcate the flame front and understand its behavior.

Total heat release rate (HRR_T): This is the total amount of heat released over the domain.

Ignition time and extinction time: The quantity HRR_T explained above varies with time, and thus the ignition time is defined as the time when HRR_T reaches the maximum value before the flame stabilizes. Similarly, the time at which HRR_T becomes minimal (near-zero) is defined as the extinction time.

Ignition location and length: These quantities are defined based on the temperature distribution in the simulation domain at the time of ignition.

Stabilization location and flame span: These quantities are defined using the axial temperature distribution after the flame stabilizes.

FREI and FREI period: For lower inlet velocities, flame extinction is followed by ignition. This kind of flame is known as the FREI. For these cases, the time required for a flame to gain two consecutive ignition incidents is defined as the FREI period (τ_{FREI}).

How these metrics are obtained and what they represent physically are elaborated in Section 3.

3. Results and Discussion

In this section, various combustion phenomena, such as ignition, stable/unstable flame behaviors, and the impacts of various operating conditions (such as the flow rate and the fuel composition) on such characteristics, are analyzed.

3.1. Ignition Process

The ignition process, which showed similar behavior for all the simulation runs, was analyzed as follows: when a syngas/air mixture flows in the channel with an inlet temperature of 300 K, it is heated up due to the positive temperature gradient imposed at the wall. Such a preheating facilitates the chain-branching reactions, which trigger ignition when the temperature is sufficiently high and produce a flame kernel somewhere downstream the channel. In this work, the ignition process is characterized by the transient total heat release rate in the domain, HRR_T , which is calculated by integrating the local heat of reaction in the computational domain at each time step,

$$HRR_T = \sum_m HRR = \sum_m \sum_n \dot{h}_r, \quad (11)$$

where m is the number of cells in the domain and n is the number of species. Because HRR_T varies with time, the ignition time is defined as the time at which HRR_T peaks,

$$t_{ig} = t_{(HRR_T)_{max}}. \quad (12)$$

Similarly, the extinction time is defined as the time at which HRR_T falls to near-zero,

$$t_{ex} = t_{(HRR_T=0)}. \quad (13)$$

This is further explained by Figure 4, associated with the inlet velocity of 1 m/s and the mixture composition A, where the time evolution of HRR_T is used to determine the ignition time. Figure 5 complements Figure 4 for further explanation of the ignition process. Here, the temperature contour plots for the selected time steps in Figure 4 are provided. Specifically, the chain branching reaction starts at time (a) and goes through time (b), indicating the beginning of the ignition process. At time (b), HRR_T of this system is maximal, and a flame front is formed, separating the unburnt and burnt mixtures. State (b) determines the ignition time (t_{ig}). From time (b) to time (c), the flame starts propagating upstream until it either becomes stable or is extinguished, depending on the boundary conditions, which are discussed in the next sections.

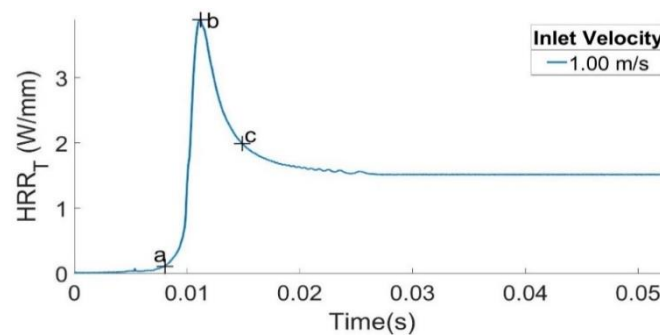


Figure 4. The total heat release rate (HRR_T) vs. time for mixture A with the inlet velocity of 1.0 m/s. The markers (a), (b) and (c) indicate selected time steps for further explanation in Figure 5.

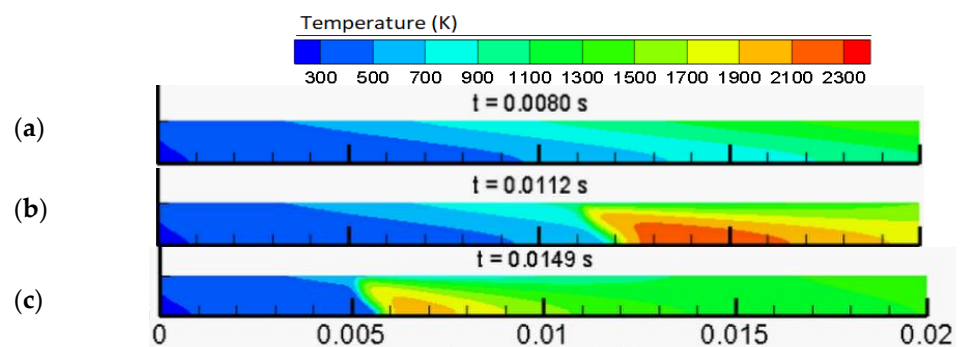


Figure 5. The temperature distribution at the selected consecutive time steps (a)–(c) for the ignition process for mixture A with the inlet velocity of 1.0 m/s. The length is measured in meters.

In addition to the ignition time, the ignition location is another metric that was defined in this work to characterize the ignition process. The axial temperature at the ignition time is analyzed in Figure 6a, and the temperature contour during the time of ignition is presented in Figure 6b. The spans over which the positive temperature gradient peaks, to where the negative temperature gradient peaks, are defined as the ignition locations. That is, $x_{(ig-st)}$ and $x_{(ig-e)}$ indicate the points where the temperature, respectively, jumps and drops, abruptly.

$$x_{ig-st} = \left(x_{\left(\frac{dT}{dx}\right)_{max}} \right)_{t_{ig}} \quad (14)$$

$$x_{ig-e} = \left(x_{\left(\frac{dT}{dx}\right)_{min}} \right)_{t_{ig}} \quad (15)$$

Further, the difference between these two points defines the ignition length, Δx_{ig} , as

$$\Delta x_{ig} = x_{ig-st} - x_{ig-e} \quad (16)$$

3.2. Flame Behaviour

After ignition, the flame front propagates downstream. Under the operating conditions employed in this work, and as the wall temperature decreases towards the upstream, the V-shaped flame may become stable at a certain location, or it may lose its stability and go through repeated extinctions and ignitions. These types of behaviors are analyzed in detail for selected operating conditions in Sections 3.2.1 and 3.2.2. The impact of all operating conditions used in this work on the ignition process and the flame behavior are subsequently elaborated in Section 3.3.

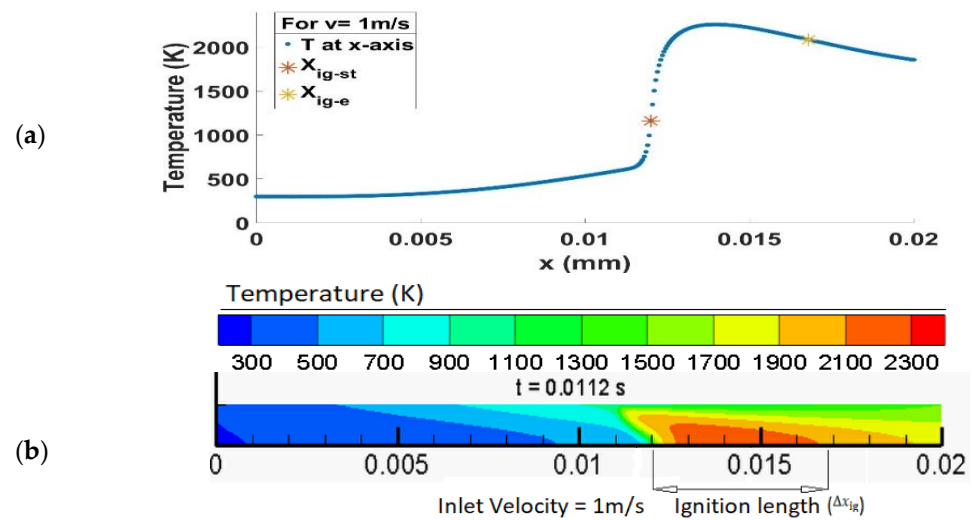


Figure 6. The temperature distribution at the time of ignition for mixture A with the inlet flow velocity of 1.0 m/s. The length is measured in meters. (a) the temperature profile along the x-axis, (b) the temperature contour in the simulation domain at the selected time step.

3.2.1. Stable Flames

In the stable modes, the flame propagates further upstream and becomes stable at a certain location. This behavior is expected in cases with higher inlet velocities (discussed in Section 3.3), in which flame propagation is balanced with the inlet velocity, resulting in a stable flame that is not too close to the inlet, where the wall temperature is sufficiently high to sustain the flame. To scrutinize this process, similar to Figures 4–6, the case with the inlet velocity of 1 m/s and the fuel mixture composition A is selected. As seen in Figure 4, HRR_T decreases after ignition until it becomes constant, indicating that the flame front has become stable. This is also confirmed by the temperature contour plots of Figure 5, where flame propagation eventually stops.

Similar to the ignition process, the properties of a stable flame front are characterized by the stabilization location. According to Figure 7, the location at which the stable flame lies is known as the stabilization location, and is obtained from the axial temperature variation in the domain for the stabilized flame. Here, the starting point of the stabilized location, $x_{(sz-st)}$, is defined as the location at which the axial temperature grows abruptly.

$$x_{sz-st} = \left(x_{\left(\frac{dT}{dx} \right)_{max}} \right)_{t_{st}} \quad (17)$$

Similarly, the ending point of the stabilized flame, $x_{(sz-e)}$, is the locus with the least temperature gradient,

$$x_{sz-e} = \left(x_{\left(\frac{dT}{dx} \right)_{min}} \right)_{t_{st}} \quad (18)$$

It is recalled that both these points are obtained at the time t_{st} , when the solution is converged and the flame front is stabilized. The difference between these points defines the flame length after the flame stabilization,

$$\Delta x_{sz} = x_{sz-st} - x_{sz-e} \quad (19)$$

3.2.2. Flames with Repeated Extinctions and Ignitions (FREI)

Under some operating conditions, the flame does not stabilize after the ignition, i.e., as it propagates further upstream, towards the inlet, the temperature is not high enough for the reactions to be sustained, so the flame is extinguished. However, with the continuous supply at the inlet, the fuel-air mixture subsequently reaches the high-temperature zone and the flame is ignited again. Such a repetitive scenario has been observed, both compu-

tationally and experimentally, and is referred to as flames with repetitive extinctions and ignitions (FREIs) in the literature [20,25,30]. To further understand this process, one of the operating conditions resulting in such a behavior is chosen (mixture A; the inlet velocity of 0.2 m/s), with the corresponding metrics elaborated.

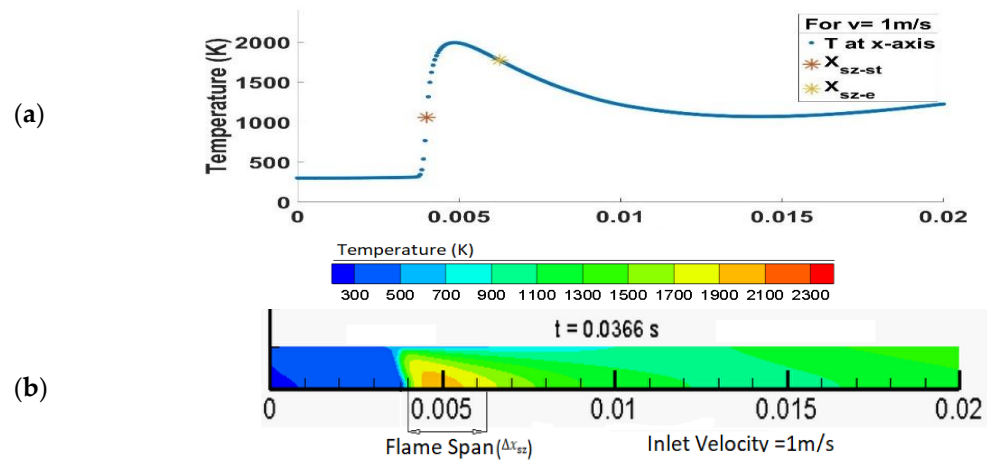


Figure 7. The temperature distribution for the stabilized flame for mixture A with the inlet flow velocity of 1.0 m/s. The length is measured in meters. (a) the temperature distribution along the x-axis, (b) the temperature contour in the simulation domain at the selected time step.

Figure 8 illustrates the variations of HRR_T , accompanied by the temperature contours of Figure 9, which correspond to the selected time steps of Figure 8. States (a)–(c) describe the ignition process discussed earlier in Section 3.1. Once ignition is completed, the flame starts propagating upstream, from state (c) to state (d). In contrast to the stable mode, the flame front does not stabilize here and continues propagating further towards the inlet, where the wall temperature is not high enough to sustain a flame. Consequently, HRR_T drops to zero and extinction occurs in state (e). With the continuous premixed fuel-air flow at the inlet, the premixture ignites again as observed between states (e) and (f). The flame is then extinguished again, from state (f) to state (h). This repeats periodically. That is, at lower inlet velocities, the flame propagation speed will not be balanced by the inlet velocity, resulting in a flame propagating farther upstream. Because the flame is closer to the inlet, where the wall temperature is not high enough, the heat transfer rates are not balanced, the flame extinguishes, and the FREI phenomenon happens.

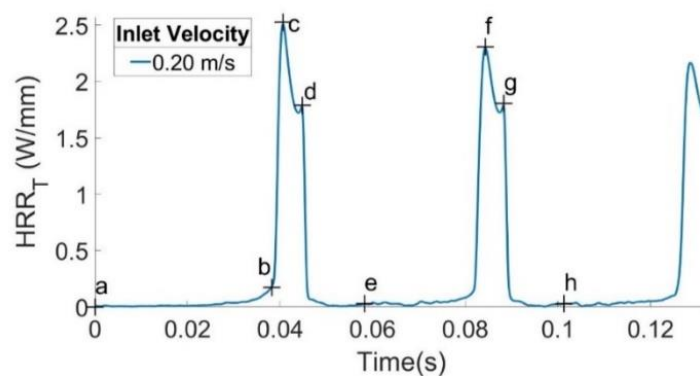


Figure 8. The total heat release rate (HRR_T) vs. time for a flame with FREI mode for mixture A with the inlet velocity of 0.2 m/s. The markers (a) to (h) indicate selected time steps for further explanation of the FREI phenomenon in Figure 9.

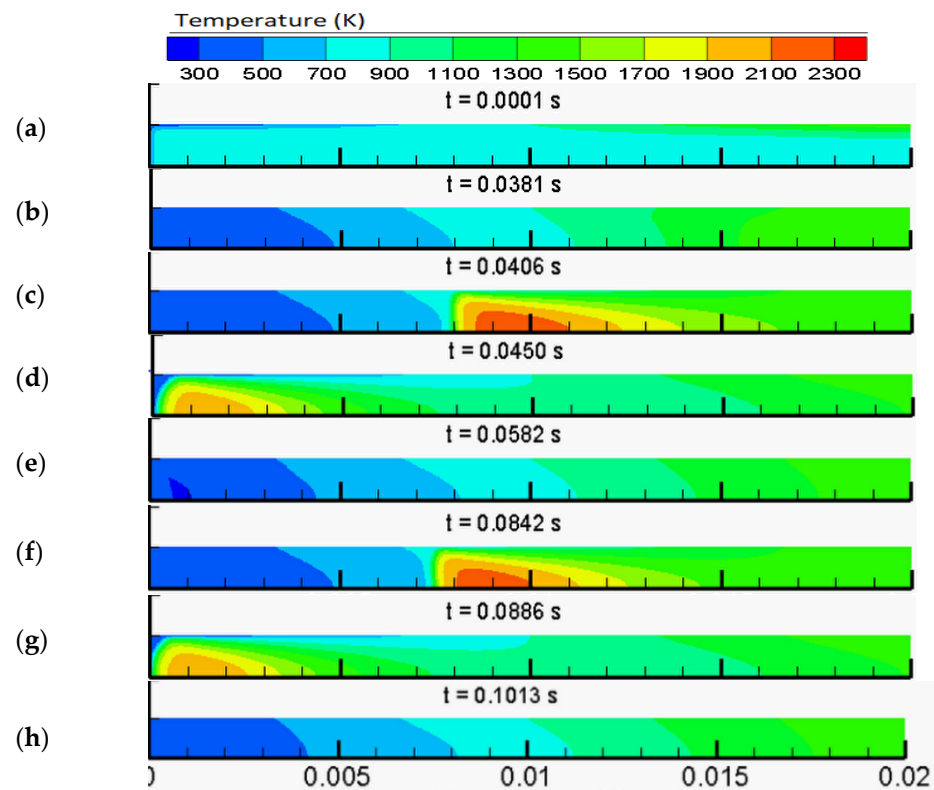


Figure 9. The temperature contours at the selected time steps for a flame with FREI mode for mixture A with the inlet velocity of 0.2 m/s. The length is measured in meters. The snapshots (a)–(h) correspond to the respective markers in Figure 8 for the selected time steps.

3.3. Impacts of Operating Conditions

The aim of the previous Sections 3.1 and 3.2 was to scrutinize the ignition process, in addition to the stable and FREI modes of syngas combustion after ignition, with the corresponding metrics defined and elaborated for a number of the cases selected from the simulation runs performed in this work. A comprehensive and fundamental understanding of how these syngas combustion properties could be altered due to slight variations in the operating conditions will help researchers and industries make more informed decisions before spending time and money on prototypes and tests. In this subsection, these characteristics are analyzed over a range of operating conditions by varying the flow rate and the syngas fuel composition.

Findings from this subsection are essentially important in understanding how changing the fuel composition or the fuel/air mixture flow rate could impact the important combustion properties, such as the ignition time/delay, the ignition location, the flame location, and the flame stability.

3.3.1. Impact of the Flow Rate (Inlet Velocity)

Various inlet velocities, in the range from 0.1 m/s to 3.0 m/s, were used to design a total of eight (8) different cases and characterize the impact of the flow rate on ignition and the flame behavior. The ignition properties, such as the ignition time, the ignition locations, and the ignition length, defined in Section 3.1, were computed for each of these eight cases and are listed in Table 2. It is shown that the ignition time is smaller for the higher inlet velocities, which is attributed to lower residence times for higher velocities (the fuel-air mixture reaches the temperatures, required for autoignition, faster). It should be noted that the ignition times/delays presented in this work are of the order of 10 ms (from 5 to 80 ms), whereas the selected time step in the simulations is 10 μ s, i.e., three orders of magnitude smaller than the ignition times, which makes it sufficiently fine to resolve the ignition time in all cases. In addition, although, to the best of our knowledge, there are no experimental

studies employing the same operating conditions as this work, the ignition times in this work are qualitatively comparable (being of the same order of magnitude) with the syngas ignition delays existing in the literature [47].

Table 2. Ignition metrics against inlet velocity for fuel mixture A.

Inlet Velocity (m/s)	Ignition Time (ms)	Ignition Location (mm)		Ignition Length (mm)
	t_{ig}	x_{ig-st}	x_{ig-e}	Δx_{ig}
0.10	77.14	6.35	9.70	3.35
0.15	52.49	6.45	9.80	3.35
0.20	40.56	7.95	11.60	3.65
0.50	18.96	9.95	13.60	3.65
0.75	13.73	12.00	16.00	4.00
1.00	11.17	12.00	16.80	4.80
1.50	8.32	13.60	19.30	5.70
3.00	5.25	16.00	20.00	4.00

The values of the ignition locations x_{ig-st} and x_{ig-e} indicate that, at higher inlet velocities, the ignition kernel appears further downstream. Moreover, it is shown that the ignition length also correlates with the inlet velocity such that the higher the velocity, the larger the ignition length. Consequently, the mixture requires higher temperatures and reaction areas to ignite at higher inlet velocities.

After completion of the ignition process, the flame behavior and stability were also found to depend on the inlet velocity. The results are presented in Figure 10, which shows a stable flame mode for the intermediate and higher inlet velocities (exceeding 0.2 m/s). For such stable flames, similar to the ignition time, the time required for the flame to stabilize also significantly decreases with the inlet flow velocity. In addition to the stabilization time, the stabilization location and the flame span (x_{sz-st} , x_{sz-e} , Δx_{sz}) were also obtained and compared in Table 3. It is shown that for higher inlet velocities, the stable flame (i) is eventually positioned further away from the inlet, and (ii) has a larger span.

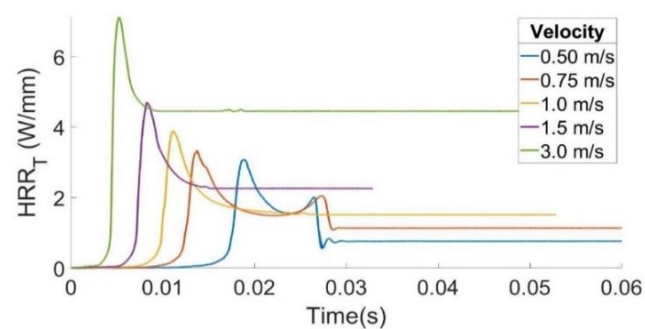


Figure 10. The total heat release rate (HRR_T) vs. time for mixture A with the inlet velocities resulting in a stable mode.

As mentioned previously, in some cases, the flame may not end up in a stable location after ignition is completed. Here, with smaller inlet velocities (≤ 0.2 m/s), the flame experiences a FREI mode. These cases with the FREI mode are further analyzed by comparing their FREI time periods, τ_{FREI} , in Table 4. It is shown that τ_{FREI} remains the same for each given inlet velocity, but diminishes with the reduction in the inlet velocity.

Table 3. The stabilization location for the stable cases for fuel mixture A.

Inlet Velocity (m/s)	Flame Location (mm)		Flame Span (mm)
	x_{sz-st}	x_{sz-e}	Δx_{sz}
0.50	0.10	1.85	1.75
0.75	0.10	2.35	2.25
1.00	4.00	6.25	2.25
1.50	7.05	9.70	2.65
3.00	10.70	15.35	4.65

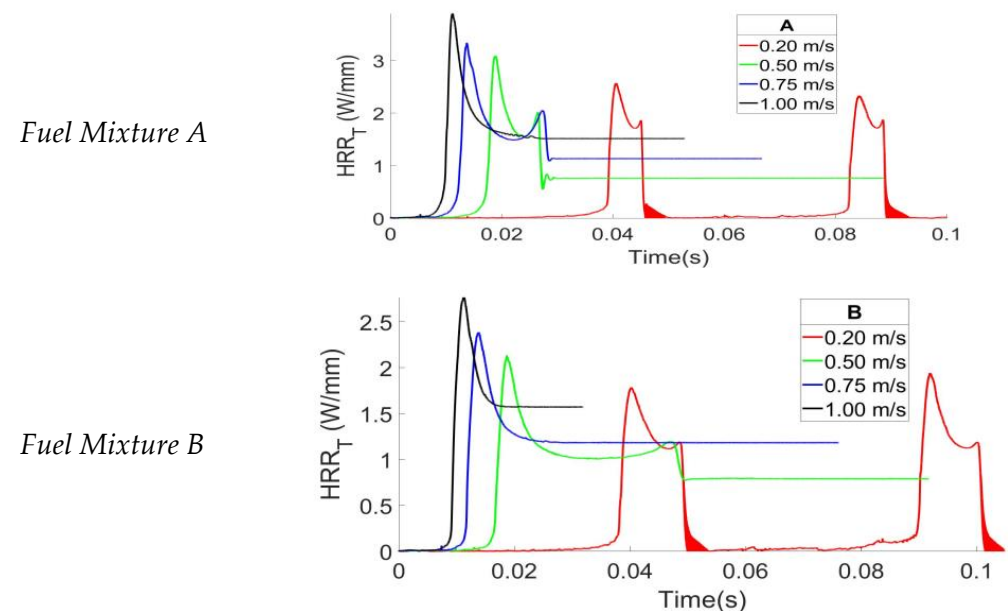
Table 4. The FREI period for the corresponding inlet velocities for fuel mixture A.

Inlet Velocity (m/s)	0.10	0.15	0.20
τ_{FREI} (ms)	82.27	55.93	42.00

3.3.2. Impact of Fuel Composition

In this section, the impact of the syngas mixture composition on the ignition and the flame behavior is analyzed. In particular, three various syngas mixtures of Table 1 are studied over various inlet flow velocities, ranging from 0.2 to 1.0 m/s. Therefore, a total of twelve cases are studied.

Figure 11 presents the time variations of HRR_T for fuel mixtures A, B, and C at various inlet flow velocities, in which both the stable flames and the FREI are observed for the lower inlet velocities for all three mixtures under consideration. As the inlet velocity exceeds 0.2 m/s, the corresponding flame stabilizes. However, the combustion characteristics are found to depend on both the fuel composition and the inlet velocity.

**Figure 11.** Cont.

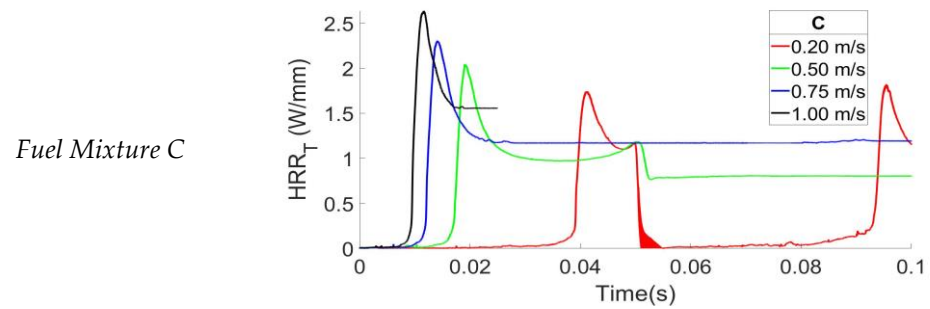


Figure 11. The total heat release rate (HRR_T) vs. time for the syngas mixtures from Table 1 at various inlet velocities.

In general, the ignition time increases as the inlet velocity decreases; see Table 5. Although the ignition time does not vary much between various fuel mixtures, the ignition length is found to be very sensitive to the fuel composition. For example, for any given inlet velocity, the ignition length, Δx_{ig} , is larger for the fuel mixture A compared to that for mixture C, and such a correlation is not observed for mixture B. Similarly, for the ignition location, ignition occurred further from the inlet for the higher inlet velocities in each case, i.e., it occurs at the locus, where the temperature of the unburnt mixture is higher due to the imposed temperature gradient at the wall. The ignition location is further from the inlet for mixtures B and C compared to mixture A.

Table 5. The ignition time and location for all cases.

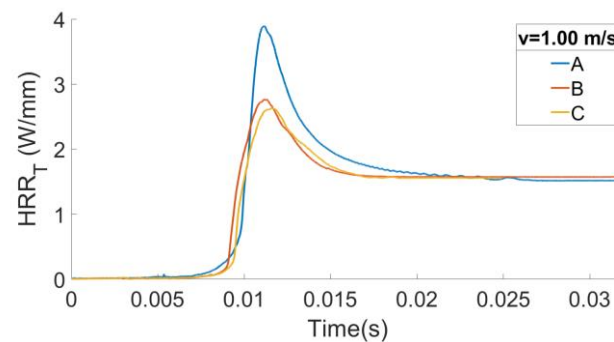
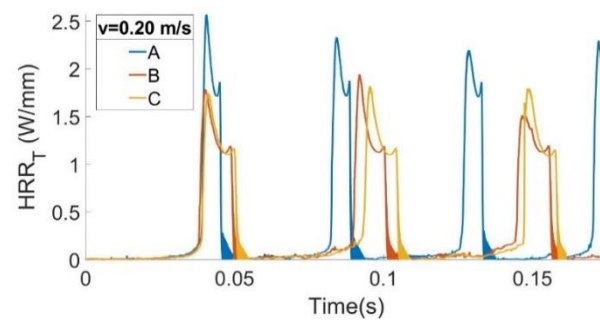
	Velocity (m/s)	t_{ig} (ms)	x_{ig-st} (mm)	x_{ig-e} (mm)	Δx_{ig} (mm)
Mixture A	0.2	40.56	7.95	11.60	3.65
	0.5	18.96	9.95	13.60	3.65
	0.75	13.73	12.00	16.00	4.00
	1.0	11.17	12.00	16.80	4.80
Mixture B	0.2	40.19	8.75	12.20	3.45
	0.5	18.66	11.35	15.50	4.15
	0.75	13.80	12.15	15.80	3.65
	1.0	11.31	12.75	16.80	4.05
Mixture C	0.2	41.20	9.15	12.15	3.00
	0.5	19.15	10.35	13.80	3.45
	0.75	14.15	12.80	16.55	3.75
	1.0	11.65	13.30	17.70	4.40

Table 6 summarizes the combustion characteristics in the cases when the stable flame has been observed. Here, the stable flame locations for these cases are compared in terms of their $x_{(sz-st)}$, which is found to be larger for mixture C compared to the other two mixtures for any given inlet velocity, whereas it is larger for mixture B compared to A. However, the difference between mixtures A and B exceeds that between mixtures B and C. The same tendency is also seen for $x_{(sz-e)}$. Further, for mixture A, in addition to the flame being stabilized closer to the inlet, it is also observed to have a shorter flame span than the other two mixtures for any given inlet velocity. The fact that these combustion metrics of mixture A differ substantially from those of mixtures B and C, while the difference between the combustion characteristics of mixtures B and C is less profound, is attributed to the higher percentage of H_2 in mixture A, which plays a major role in controlling the stable flame location and length.

Table 6. The location of the stabilized flame.

	Velocity (m/s)	x_{sz-st} (mm)	x_{sz-e} (mm)	Δx_{sz} (mm)
Mixture A	0.5	0.10	1.85	1.75
	0.75	0.10	2.35	2.25
	1.0	4.00	6.25	2.25
Mixture B	0.5	0.10	2.20	2.10
	0.75	7.15	9.40	2.25
	1.0	9.15	11.60	2.45
Mixture C	0.5	0.10	2.20	2.10
	0.75	7.50	9.65	2.15
	1.0	9.50	12.00	2.50

To further study the impact of syngas composition on the flame behavior, the quantities HRR_T are compared for all three mixtures at two inlet velocities. First, we chose the inlet velocity of 1.0 m/s, where all three mixtures resulted in stable flames, see Figure 12. Here, mixture A (containing 65% of H_2) provides the largest HRR_T peak compared to the other two mixtures, thereby showing the high energy density of H_2 . In addition, it took longer for the flame to be stabilized for mixture A compared to mixtures B and C. Second, we chose the inlet velocity of 0.2 m/s, where the FREI phenomenon was observed for all three mixtures, see Figure 13. Specifically, the time evolution of HRR_T is depicted in Figure 13 for mixtures A, B, and C, thereby representing the unstable cases, in which each ignition is followed by the extinction, in a repetitive manner.

**Figure 12.** The total heat release rate (HRR_T) vs. time for the stable flame cases with the inlet velocity of 1.0 m/s.**Figure 13.** The total heat release rate (HRR_T) vs. time for the FREI cases with the inlet velocity of 0.2 m/s.

These repetitive ignition times are given in Table 7 for all cases. Here, t_{ig-x} represents the x^{th} ignition time, and $t_{ig-y,x}$ represents the difference between the y^{th} and x^{th} ignition

times. It is observed that the consecutive ignition time remains almost the same for each case, with a slight discrepancy that can be attributed to numerical artifacts. However, the FREI cases for mixture A show a higher maximum heat release rate compared to those of mixtures B and C, which can be attributed to a higher hydrogen composition in mixture A because H_2 possesses higher energy density. Similarly, it is seen that τ_{FREI} is smaller for mixture A. Thus, the burning process of mixture A can be regarded as an oscillating flame. However, τ_{FREI} increases for mixture B by 2.0 ms, whereas for mixture C, τ_{FREI} decreases by 2.0 ms, which cannot be ignored. As we know, mixture C differs from the other two mixtures in terms of the CO percentage (i.e., it has almost twice the amount of the other two). Thus, we can suggest that this significantly higher percentage of CO in mixture C reduces τ_{FREI} , causing the FREI incident to occur more quickly. Among the two mixtures having the same CO percentage (A and B), mixture B has a higher percentage of CH_4 and a lower percentage of H_2 ; thus, for mixture B, τ_{FREI} is observed to be larger by 2.0 ms. A similar trend can be seen when comparing mixtures C and A. It is observed that although CH_4 and H_2 are the main driving forces to generate the FREI behavior, a CO fraction in the fuel mixture plays an important role in controlling the FREI frequency.

Table 7. Ignition time for the FREI cases given in Figure 13.

	t_{ig-1} (ms)	t_{ig-2} (ms)	t_{ig-3} (ms)	$\Delta t_{ig-2,1}$ (ms)	$\Delta t_{ig-3,2}$ (ms)
Mixture A	40.4	84.3	128.6	43.9	44.3
Mixture B	40.2	92.0	146.5	51.8	54.5
Mixture C	41.3	95.6	148.2	54.3	52.6

4. Conclusions

In this work, microscale combustion of syngas mixtures was studied, computationally, with the use of detailed chemical kinetics. The key agent of conjugate wall heat loss, which is inherent to microscale combustion, was addressed by imposing a temperature gradient on the wall, which also preheated the fuel mixture. The flame dynamics and other combustion characteristics at microscales were studied for various inlet flow velocities (ranging from 0.1 to 3.0 m/s) and syngas compositions (mixture A: 30% CO, 5% CH_4 , and 65% H_2 ; mixture B: 70% CO, 5% CH_4 , and 25% H_2 ; and mixture C: 60% CO, 10% CH_4 , and 30% of H_2). Two different phenomena—the stable flames and the FREI—were observed with respect to the inlet velocities, such that for high inlet velocities ranging from 0.5 to 3.0 m/s, the flame was stable, whereas for the velocity range from 0.1 to 0.2 m/s, the flame became unstable and the FREI was observed. The ignition time, ignition location, and ignition length were analyzed for each case, and the stabilization characteristics, such as the stabilized flame location for the stable flames, were scrutinized. The ignition time and location, in addition to the stabilized flame location, where maximum domain temperatures are expected, are significantly important factors in designing micro-combustion-related technologies with syngas as a fuel. In particular, conjugate heat transfer/heat losses play an important role in micro-combustion devices, in which the ratio of the surface area to the volume is relatively higher than that of the conventional combustion devices. Further, the FREI properties were calculated and compared for the unstable cases. Regarding the fuel mixture composition, in the stable cases, mixture A showed more variations in terms of the total heat release, stabilization time, flame location, and flame span compared to those in mixtures B and C. Similarly, for the unstable cases, the time difference between the consecutive ignitions varied for all of the cases. Mixture A, which had a higher percentage of H_2 , was found to have a higher total heat release in the domain, and significantly different characteristics compared to the other two mixtures. This corroborates the major role and dominance of an H_2 fraction in syngas combustion. Similarly, the effect of CO can be projected in the FREI mode for mixtures B and C in terms of the FREI period (τ_{FREI}). From a practical perspective, because syngas is generated from a variety of sources and methodologies, and can consist of different species of a wide range of concentrations, the

findings of this work are critically important in selecting the appropriate composition of syngas depending on the application.

This research can be further extended in the following directions:

- (a) to conduct in situ experiments for the operating conditions used in this work;
- (b) to study the impact of the equivalence ratio on the flame behavior and instabilities;
- (c) to consider 3D geometries and compare the results with those from 2D simulations; and
- (d) to study the geometrical impacts on syngas combustion at microscales, while undertaking both experimental and numerical analyses over different geometries.

Author Contributions: Conceptualization, M.A. and V.A.; Data curation, S.P., M.A. and V.A.; Formal analysis, S.P., M.A. and V.A.; Funding acquisition, S.P., M.A. and V.A.; Investigation, S.P., M.A. and V.A.; Methodology, S.P., M.A. and V.A.; Project administration, M.A. and V.A.; Resources, V.A.; Software, S.P.; Supervision, M.A. and V.A.; Validation, S.P. and M.A.; Visualization, S.P.; Writing—original draft, S.P.; Writing—review & editing, M.A. and V.A. All authors have read and agreed to the published version of the manuscript.

Funding: The work at West Virginia University was supported by the National Science Foundation (NSF), through CAREER Award #1554254 (V.A.), as well as by West Virginia Higher Education Policy Commission, through Grant #HEPC.dsr.18.7 (V.A.). Wayne State University’s Research reported in this publication was supported in part by funding provided by the National Aeronautics and Space Administration (NASA), under award number 80NSSC20M0124, Michigan Space Grant Consortium (MSGC).

Institutional Review Board Statement: Not applicable.

Informed Consent Statement: Not applicable.

Data Availability Statement: The data presented in this study are available on request from the corresponding author.

Conflicts of Interest: The authors declare no conflict of interest.

References

1. Chen, W.L.; Huang, C.W.; Li, Y.-H.; Kao, C.-C.; Cong, H.T. Biosyngas-fueled platinum reactor applied in micro combined heat and power system with a thermophotovoltaic array and Stirling engine. *Energy* **2020**, *194*, 116862. [[CrossRef](#)]
2. Yang, W.M.; Chou, S.K.; Shu, C.; Xue, H.; Li, Z.W.; Li, D.T.; Pan, J.F. Microscale combustion research for application to micro thermophotovoltaic systems. *Energy Convers. Manag.* **2003**, *44*, 2625–2634. [[CrossRef](#)]
3. Fernandez-Pello, A. Micropower generation using combustion: Issues and approaches. *Proc. Combust. Inst.* **2002**, *29*, 883–899. [[CrossRef](#)]
4. Kaisare, N.; Vlachos, D. A review on microcombustion: Fundamentals, devices and applications. *Prog. Energy Combust. Sci.* **2012**, *38*, 321–359. [[CrossRef](#)]
5. Walther, D.C.; Ahn, J. Advances and challenges in the development of power-generation systems at small scales. *Prog. Energy Combust. Sci.* **2011**, *37*, 583–610. [[CrossRef](#)]
6. Ju, Y.; Maruta, K. Microscale combustion: Technology development and fundamental research. *Prog. Energy Combust. Sci.* **2011**, *37*, 669–715. [[CrossRef](#)]
7. Wang, Z.; Bai, Z.; Yu, G.; Yelishala, S.; Metghalchi, H. The critical pressure at the onset of flame instability of syngas/air/diluent outwardly expanding flame at different initial temperatures and pressures. *J. Energy Resour. Technol.* **2019**, *141*, 082207. [[CrossRef](#)]
8. Ali, K.; Kim, C.; Lee, Y.; Oh, S.; Kim, K. A Numerical study to investigate the effect of syngas composition and compression ratio on the combustion and emission characteristics of a syngas-fueled HCCI engine. *J. Energy Resour. Technol.* **2020**, *142*, 092301. [[CrossRef](#)]
9. Islam, S.; Dincer, I. A comparative study of syngas production from two types of biomass feedstocks with waste heat recovery. *J. Energy Resour. Technol.* **2018**, *140*, 092002. [[CrossRef](#)]
10. Al-Zareer, M.; Dincer, I.; Rosen, M.A. Influence of selected gasification parameters on syngas composition from biomass gasification. *J. Energy Resour. Technol.* **2018**, *140*, 041803. [[CrossRef](#)]
11. Liu, X.; Burra KR, G.; Wang, Z.; Li, J.; Che, D.; Gupta, A.K. Syngas characteristics from catalytic gasification of polystyrene and pinewood in CO₂ atmosphere. *J. Energy Resour. Technol.* **2021**, *143*, 052304. [[CrossRef](#)]
12. Ayooobi, M.; Schoegl, I. Non-catalytic conversion of glycerol to syngas at intermediate temperatures: Numerical methods with detailed chemistry. *Fuel* **2017**, *195*, 190–200. [[CrossRef](#)]
13. Othman, N.F.; Boosroh, M.H. Effect of H₂ and CO contents in syngas during combustion using Micro Gas Turbine. In *IOP Conference Series: Earth and Environmental Science*; IOP Publishing: Bristol, UK, 2016; Volume 32.

14. Pio, G.; Ricca, A.; Palma, V.; Salzano, E. Experimental and numerical evaluation of low-temperature combustion of bio-syngas. *Int. J. Hydrog. Energy* **2020**, *45*, 1084–1095. [[CrossRef](#)]
15. Salzano, E.; Basco, A.; Cammarota, F.; Di Sarli, V.; Di Benedetto, A. Explosions of Syngas/CO₂ mixtures in oxygen-enriched air. *Ind. Eng. Chem. Res.* **2012**, *51*, 7671–7678. [[CrossRef](#)]
16. Xie, Y.; Wang, J.; Cai, X.; Huang, Z. Pressure history in the explosion of moist syngas/air mixtures. *Fuel* **2016**, *185*, 18–25. [[CrossRef](#)]
17. Sun, Z.Y. Laminar explosion properties of syngas. *Combust. Sci. Technol.* **2018**, *192*, 166–181. [[CrossRef](#)]
18. Mardani, A.; Mahalegi HK, M. Hydrogen enrichment of methane and syngas for MILD combustion. *Int. J. Hydrog. Energy* **2019**, *44*, 9423–9437. [[CrossRef](#)]
19. Zhang, K.; Jiang, X. Uncertainty quantification of fuel variability effects on high hydrogen content syngas combustion. *Fuel* **2019**, *257*, 116111. [[CrossRef](#)]
20. Dam, B.; Ardha, V.; Choudhuri, A. Laminar flame velocity of syngas fuels. *J. Energy Resour. Technol.* **2010**, *132*, 044501. [[CrossRef](#)]
21. Monteiro, E.; Rouboa, A. Measurements of the laminar burning velocities for typical syngas-air mixtures at elevated pressures. *J. Energy Resour. Technol.* **2011**, *133*, 031002. [[CrossRef](#)]
22. Wei, L.; Pordesimo, L.O.; Filip To, S.D.; Herndon, C.W.; Batchelor, W.D. Evaluation of micro-scale syngas production costs through modeling. *Trans. ASABE* **2009**, *52*, 1649–1659. [[CrossRef](#)]
23. Maruta, K.; Kataoka, T.; Kim, N.; Minaev, S.; Fursenko, R. Characteristics of combustion in a narrow channel with a temperature gradient. *Proc. Combust. Inst.* **2005**, *30*, 2429–2436. [[CrossRef](#)]
24. Brambilla, A.; Schultze, M.; Frouzakis, C.E.; Mantzaras, J.; Bombach, R.; Boulouchos, K. An experimental and numerical investigation of premixed syngas combustion dynamics in mesoscale channels with controlled wall temperature profiles. *Proc. Combust. Inst.* **2015**, *35*, 3429–3437. [[CrossRef](#)]
25. Resende, P.R.; Ayoobi, M.; Afonso, A. Numerical investigations of micro-scale diffusion combustion: A Brief Review. *Appl. Sci.* **2019**, *9*, 3356. [[CrossRef](#)]
26. Akkerman, V.; Bychkov, V.; Petchenko, A.; Eriksson, L.-E. Flame oscillations in tubes with nonslip at the walls. *Combust. Flame* **2006**, *145*, 675–687. [[CrossRef](#)]
27. Ayoobi, M.; Schoegl, I. Numerical analysis of flame instabilities in narrow channels: Laminar premixed methane/air combustion. *Int. J. Spray Combust. Dyn.* **2017**, *9*, 155–171. [[CrossRef](#)]
28. Resende, P.R.; Afonso, A.; Pinho, C.; and Ayoobi, M. Impacts of Dilution on Hydrogen Combustion Characteristics and NO_x Emissions. *ASME J. Heat Transfer* **2019**, *141*, 012003. [[CrossRef](#)]
29. Zhang, Z.; Wu, K.; Yao, W.; Yuen, R.; Wang, J. Enhancement of combustion performance in a microchannel: Synergistic effects of bluff-body and cavity. *Fuel* **2020**, *265*, 116940. [[CrossRef](#)]
30. Malushte, M.; Kumar, S. Flame dynamics in a stepped micro-combustor for non-adiabatic wall conditions. *Therm. Sci. Eng. Prog.* **2019**, *13*, 100394. [[CrossRef](#)]
31. Pizza, G.; Frouzakis, C.E.; Mantzaras, J.; Tomboulides, A.G.; Boulouchos, K. Dynamics of premixed hydrogen/air flames in microchannels. *Combust. Flame* **2008**, *152*, 433–450. [[CrossRef](#)]
32. Kim, N.; Maruta, K. A numerical study on propagation of premixed flames in small tubes. *Combust. Flame* **2006**, *146*, 283–301. [[CrossRef](#)]
33. Norton, D.G.; Vlachos, D.G. Combustion characteristics and flame stability at the microscale: A CFD study of premixed methane/air mixtures. *Chem. Eng. Sci.* **2003**, *58*, 4871–4882. [[CrossRef](#)]
34. Munir, F.A.; Mikami, M. A numerical study of propane-air combustion in meso-scale tube combustors with concentric rings. *J. Therm. Sci. Technol.* **2015**, *10*, JTST0008. [[CrossRef](#)]
35. Konakov, S.A.; Dzyubanenko, S.V.; Krzhizhanovskaya, V.V. Computer simulation approach in development of propane-air combustor microreactor. *Procedia Comput. Sci.* **2016**, *101*, 76–85. [[CrossRef](#)]
36. Wang, W.; Zuo, Z.; Liu, J. Experimental study and numerical analysis of the scaling effect on the flame stabilization of propane/air mixture in the micro-scale porous combustor. *Energy* **2019**, *174*, 509–518. [[CrossRef](#)]
37. Takbiri-Borujeni, A.; Ayoobi, M. Application of physics-based machine learning in combustion modeling. In Proceedings of the 11th US National Combustion Meeting, Pasadena, CA, USA, 24–27 March 2019.
38. Pokharel, S.; Ayoobi, M.; Akkerman, V. Characterizing premixed syngas combustion and flame dynamics in micro scales. In Proceedings of the 2020 28th Conference on Nuclear Engineering Joint with the ASME 2020 Power Conference ICONE28-POWER2020, Virtual Conference, 4–5 August 2020; pp. 1–7. Available online: <https://event.asme.org/POWER-2020> (accessed on 10 July 2021).
39. Kousheshi, N.; Yari, M.; Paykani, A.; Mehr, A.S.; de la Fuente, G.F. Effect of syngas composition on the combustion and emissions characteristics of a syngas/diesel RCCI engine. *Energies* **2020**, *13*, 212. [[CrossRef](#)]
40. Chuahy, F.D.F.; Kokjohn, S.L. High efficiency dual-fuel combustion through thermochemical recovery and diesel reforming. *Appl. Energy* **2017**, *195*, 503–522. [[CrossRef](#)]
41. Maruta, K.; Parc, J.K.; Oh, K.C.; Fujimori, T.; Minaev, S.S.; Fursenko, R.V. Characteristics of microscale combustion in a narrow heated channel. *Combust. Explos. Shock Waves* **2004**, *40*, 516–523. [[CrossRef](#)]
42. Baumgardner, M.E. Microreactor combustion of simple hydrocarbons. In Proceedings of the 11th U.S. National Combustion Meeting, Pasadena, CA, USA, 24–27 March 2019.

43. Di Stazio, A.; Chauveau, C.; Dayma, G.; Dagaut, P. Oscillating flames in micro-combustion. *Combust. Flame* **2016**, *167*, 392–394. [[CrossRef](#)]
44. Di Stazio, A.; Chauveau, C.; Dayma, G.; Dagaut, P. Pulsating combustion of ethylene in micro-channels with controlled temperature gradient. In *Combustion Science and Technology*; Taylor & Francis: Abingdon, UK, 2018; pp. 1–11.
45. Chemical-Kinetic Mechanisms for Combustion Applications, San Diego Mechanism, Mechanical and Aerospace Engineering (Combustion Research), University of California at San Diego. Available online: <http://combustion.ucsd.edu> (accessed on 10 July 2021).
46. ANSYS Fluent [online]. Available online: <https://www.ansys.com/products/fluids/ansys-fluent> (accessed on 10 July 2021).
47. Lee, H.C.; Jiang, L.Y.; Mohamad, A.A. A review on the laminar flame speed and ignition delay time of Syngas mixtures. *Int. J. Hydrog. Energy* **2014**, *39*, 1105–1121. [[CrossRef](#)]